Noninvasive Method for Monitoring Ethanol in Fermentation Processes Using Fiber-Optic Near-Infrared Spectroscopy

Anna G. Cavinato, David M. Mayes, Zhihong Ge, and James B. Callis*

Center for Process Analytical Chemistry, Department of Chemistry, BG-10, University of Washington, Seattle, Washington 98195

Short-wavelength near-infrared (SW-near-IR) spectroscopy (700–1100 nm) is used for the determination of ethanol during the time course of a fermentation. Measurements are performed noninvasively by means of a photodiode array spectrometer equipped with a fiber-optic probe placed on the outside of the glass-wall fermentation vessel. Pure ethanol/ water and ethanol/yeast/water mixtures are studied to establish the spectral features that characterize ethanol and to show that determination of ethanol is independent of the yeast concentration. Analysis of the second-derivative data is accomplished with multilinear regression (MLR). The standard error of prediction (SEP) of ethanol in ethanol/water solutions is approximately 0.2% over a range of 0–15%; the SEP of ethanol in ethanol/yeast/water solutions is 0.27% (w/w). Results from the mixture experiments are then applied to actual yeast fermentations of glucose to ethanol. By use of a gas chromatographic method for validation, a good correlation is found between the intensity of backscattered light at 905 nm and the actual ethanol. Additional experiments show that a calibration model created for one fermentation can be used to predict ethanol production during the time course of others with a prediction error of 0.4%.

INTRODUCTION

The need for real-time monitoring of the chemical and physiological status of fermentation processes and the lack of suitable sensors for this purpose have long been recognized (*1, 2*). For the case of alcohol fermentations, measurements are limited to the determination of physical parameters which only give indirect estimates of ethanol production. Recently, efforts have been made to develop direct analyses for ethanol in fermentation broths (*3, 4*). Unfortunately, most of these techniques require sample removal and preparation. A noninvasive method would be desirable, because sterility problems can be avoided and sampling is simplified (*2*). While there are a number of potential noninvasive analytical techniques such as X-ray, ultrasound, nuclear magnetic resonance, and infrared emission, the most readily implemented one is short-wavelength near-infrared (SW-near-IR) spectroscopy, which lies between 700 and 1100 nm (*5*). For the most part, absorptions in this spectral region arise from the second and third overtones of CH, OH, and NH stretches together with combination bands from other types of vibrations. The exact position of the bands depends on the chemical environment giving rise to a reasonably high degree of uniqueness of the spectra for different organic molecules.

Although the low extinction coefficients of these highly forbidden transitions may seem a disadvantage, they can actually be of great utility for analysis of major constituents in the 0.1–100% concentration range. First, long path lengths are used, ensuring that a spectrum is more representative of the bulk and that a thin layer of adsorbed materials on the optical window will not fatally degrade the results. Second, quantitative measurements can be made on highly scattering materials. Both diffuse transmittance and diffuse reflectance geometries can be used. Additionally, the hardware in this region is very inexpensive and employs readily available fiber-optic components, conventional monochromators, tungsten lamps, and silicon detectors. Even with use of inexpensive components, signal-to-noise ratios on the order of 10000:1 can be obtained. Thus, very subtle changes in the spectra can be reliably used for analysis. Because this sensing technology is readily implemented in multichannel form (*6*), multiple characteristics of a bioprocess can be potentially monitored simultaneously.

One apparent disadvantage of SW-near-IR spectroscopy is that the spectral resolution in condensed phase is not high enough to ensure that the absorption bands arising from the different species in a mixture will be free of interferences. This necessitates the use of multivariate statistical calibration (*7*). Results obtained by Alberti et al. (*4*) using Fourier transform infrared (FT-IR) data show the advantages of this quantitation technique. These authors measured the infrared spectra of fermentation broths and extracted quantitative information about glucose, ethanol, and glycerol, using multivariate analysis. At the Center for Process Analytical Chemistry, SW-near-IR spectroscopy and multivariate calibration have been used for gasoline quality evaluation, making simultaneous measurement of octane numbers, API density, bromine number, total aromatics, olefins, and aliphatics (*8*) and for measurement of caustic and caustic brine (*9*). Near-IR technology is well established as an analytical method in the agricultural commodities industries (*10*) and has already been used to follow solid-phase fermentations (*11*).

The above review serves as a powerful rationale for the use of the SW-near-IR spectroscopy and multivariate statistical calibration as a noninvasive means of monitoring biofermentations. In this work, the feasibility of continuous analysis of ethanol production directly through the walls of a glass fermentation vessel is demonstrated. Monitoring and control of ethanol production are of obvious interest in the beer and wine industry and distilleries. Officially, alcohol in beverages is measured by specific gravity (picnometry and hydrometry) or refractometry (*12*). Although these methods are reproducible to 0.1–0.2%, they suffer from several drawbacks such as a long and complicated analysis and large sample size (*13*). A number of other analytical methods have been proposed for determination of ethanol in beverages and fermentation broths. These include gas chromatography (*14*), Fourier transform infrared spectroscopy (*4, 15*), nuclear magnetic resonance (*16*), near-infrared spectroscopy (*17, 18*), laser Raman spectrometry (*19*), immobilized enzymes (*20, 21*), and flow injection analysis (*22, 23*). Some of these techniques do not have enough precision, while others are lengthy and/or expensive; most have no potential for noninvasive analysis.

MATERIALS AND METHODS

Biofermentation. The yeast *Saccharomyces cerevisiae* was grown anaerobically on the defined medium listed in Table I with glucose as the carbon source. The fermentation was carried out

Table I. Defined Medium for *Saccharomyces cerevisiae* Fermentation

| component	amt, g/L
glucose	150–200
yeast extract	10.4
ammonium sulfate	9.2
potassium hydrogen phosphate	2.9
magnesium sulfate	1.25

Apparatus
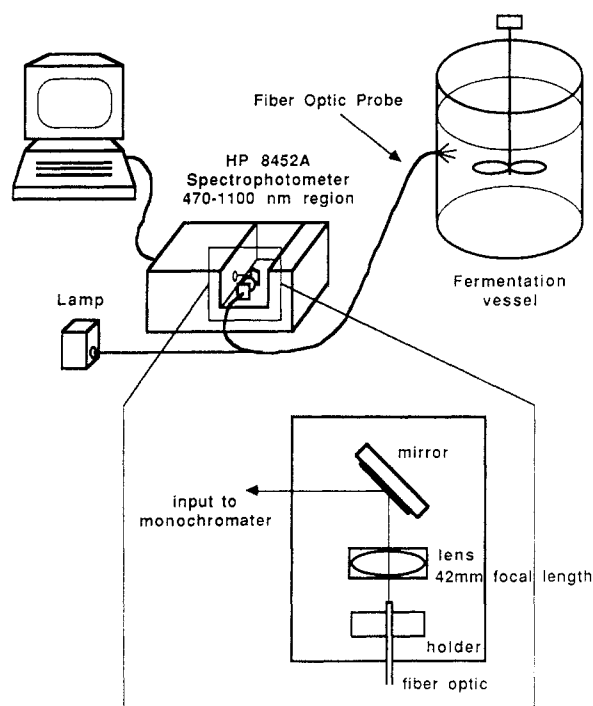
Figure 1. Schematic diagram of the instrument.

in a Bioflow I reactor from New Brunswick Scientific, Inc., of 2-L capacity. The culture was maintained at room temperature with an agitation speed of 300 rpm. Samples of 2-mL volume were withdrawn periodically for ethanol analysis by GC.

Ethanol Analysis. Ethanol analysis was performed on a Hewlett-Packard Model 5880A gas chromatograph equipped with a flame ionization detector (FID) (*24*). The column was a 6 ft × 20 mm i.d. glass 5% Carbowax 20M on 60/80 mesh Carbopack B. The chromatograph was operated under the following conditions: column temperature, 80 °C; injector temperature, 125 °C, FID temperature, 125 °C; carrier gas flow rate, 20 mL/min. The injection volume was 0.5 μL. Prior to injection, each sample was diluted with an equal volume of 2% by weight 1-propanol solution as an internal standard. The chromatograph was calibrated with aqueous ethanol samples diluted with the internal standard.

Near-IR Spectroscopy. SW-near-IR spectroscopy was carried out by means of a Hewlett-Packard 8452A photodiode array based spectrophotometer with the near-infrared option. The instrument was modified for use with a bifurcated fiber-optic probe (Sterngold Corp; 1 m in length, 6 mm outside bundle diameter, 2 mm inside bundle diameter) (Figure 1). As a light source a tungsten/halogen lamp (Osram 64635), operated from a stable dc power supply, was employed. It was focused on the outer bundle and guided to the sample. Light backscattered from the sample was collected by the inner bundle and directed to the monochromator. A 42-mm focal length asymmetric lens was used to collimate the light from the inner fiber bundle. This collimated light impinged on the collecting lens supplied by the manufacturer, which focused it on the entrance slit. With this configuration, the instrument retains the factory spectral resolution of 4 nm and a peak-to-peak
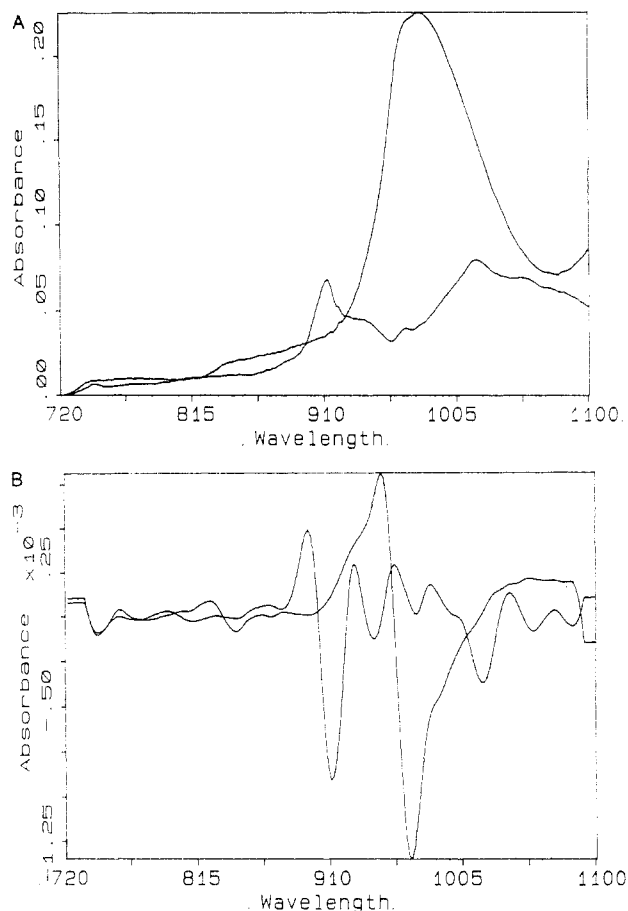
Figure 2. Absorbance spectra of pure water and pure ethanol (A). Second derivative spectra of pure water and pure ethanol (B). Spectra taken in transmission geometry in a 1-cm cuvette.

signal-to-noise ratio of 10^4:1 at zero absorbance with a 25-s averaging time and a 0.1-s acquisition time (*25*). Similar modifications of the HP8452A for use with fiber optics have been reported (*26*). The ethanol/water mixtures were analyzed in transmission mode using a 1-cm quartz absorption cell. In this configuration, an additional fiber bundle was used to convey the transmitted light to the collimating lens. The ethanol/yeast/water mixtures, as well as the fermentation, were monitored by placing the bifurcated fiber-optic probe (*6*) up to the side of a 1 × 1 × 4 cm quartz cuvette (1 cm path length) or the fermentor glass vessel wall. Spectra were obtained from the light scattered back to the fiber bundle from the scattering particles in the medium.

Data Analysis. Data analysis was carried out on an IBM PC-AT. Spectra were first smoothed and a second derivative transformation was calculated using a 26-nm window with in-house-developed software. In the analysis and comparison of spectral data from different experiments, the same smoothing and second derivative parameters were used. For calibration and prediction of ethanol content in a sample, stagewise multiple linear regression (MLR) provided by Pacific Scientific Co. (NIRS, Inc., Silver Spring, MD) was used. The standard error of prediction was from a cross validation estimate (*27*) that uses all but one sample as a calibration set to form a prediction equation, and then a prediction is made of the remaining sample. This "leave-one-out" exercise was repeated for each sample in the training set and the standard error of prediction was determined from the predicted and actual values for samples omitted.

RESULTS AND DISCUSSION

Basic Spectroscopy. The spectra of pure water and pure ethanol in the spectral region 700–1100 nm in a 1-cm cuvette are shown in Figure 2A. For water the most prominent band is at 960 nm. As previously noted (*9*) this band arises from the overtone combination motion ($2\nu_1 + \nu_3$) where ν_1 is the symmetric OH stretch and ν_3 the bending mode. The band

Figure 4. Multiple R plot vs wavelength of water/ethanol mixtures using one wavelength.
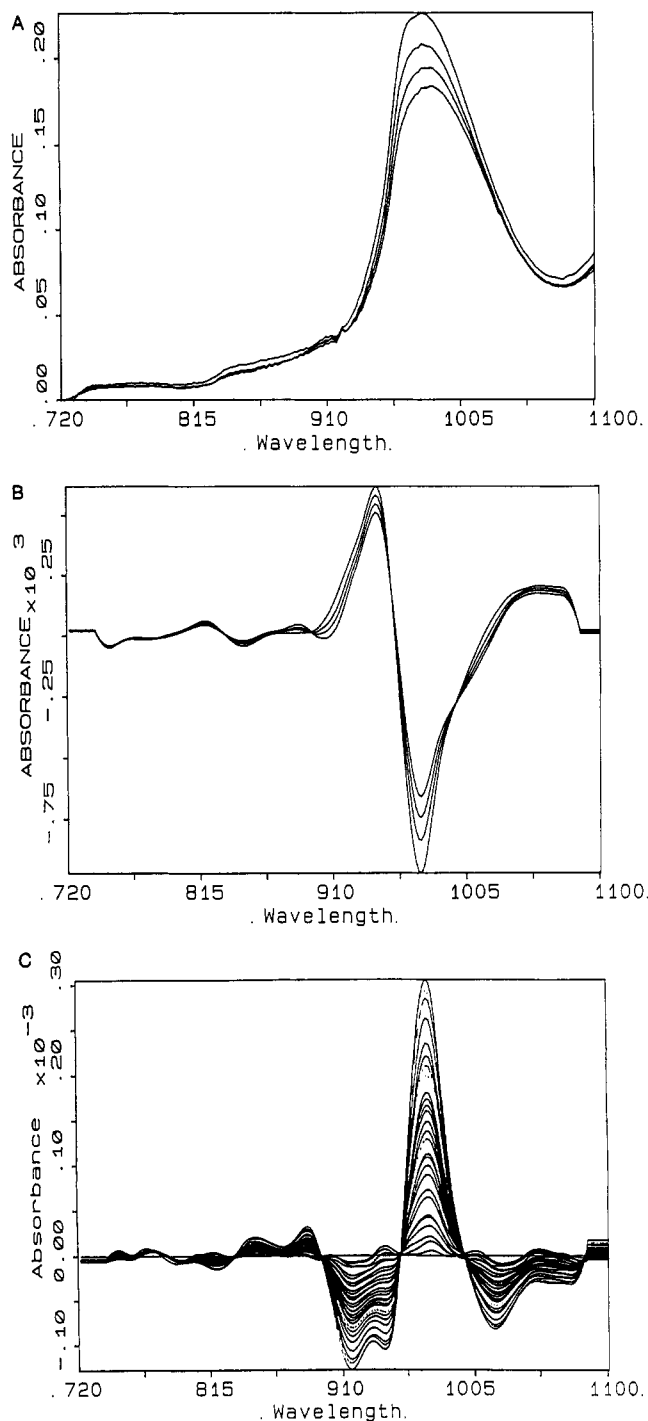
Figure 3. Absorbance spectra of water/ethanol mixtures (0–15% (w/w)) (A). Second derivative spectra of 3A (B). Second derivative difference spectra of 3B (C). Spectra taken in transmission geometry in a 1-cm cuvette.

made for hydrocarbons (29) and the ratio of intensities reflects the ratio of protons on the methyl and methylene functional groups, respectively.

Calculation of the second derivative eliminates baseline offsets due to cuvette placement in the single-beam spectrophotometer and provides better spectral resolution. The second derivative spectra of pure water and ethanol are shown in Figure 2B. The ethanol second derivative intensities are considerably increased relative to those of water. In the zero derivative spectrum the maximum extinction coefficient of water is more than 4 times that of ethanol, whereas in second derivative the absorption intensities are about equal. This is a result of the ethanol bands being sharper than those of water. In addition, the 935-nm methylene band is fully resolved from the methyl band.

Analysis of Ethanol/Water Mixtures. The basic concepts of the use of SW-near-IR spectroscopy and multivariate calibration are well illustrated by the study of simple mixtures of ethanol and water and provide a basis for analysis of the more complex fermentation broths. Accordingly, a series of ethanol/water mixtures in the 0–15% (w/w) concentration range were prepared and their spectra taken (Figure 3A). The major spectroscopic feature in this data set is the water band at 960 nm while the methyl stretch of ethanol at 905 nm is present as a minor shoulder. The artifact at 915 nm is instrumental and arises from a filter placed over the photodiode array. Oscillations in the data arise from the "odd–even" readout scheme for this detector. The disappearance of the 960-nm water band is the most prominent spectral change as a result of the dilution of water with ethanol addition. After calculation of the second derivative (Figure 3B), the methyl stretch of ethanol is much more prominent. To further enhance the spectral features for observation purposes, the second derivative spectrum of pure water is subtracted from the data set. Now, in the second derivative difference spectra (Figure 3C), both the methyl and methylene stretches are well resolved.

The second derivative spectra of the ethanol/water mixtures (Figure 3B) were analyzed by stagewise MLR. A very high correlation (correlation coefficient $R = 0.999$) was obtained with just one wavelength, 905 nm. The plot of multiple R vs wavelength (Figure 4) shows a region of high correlation corresponding to the methyl band. An additional wavelength does not improve the correlation significantly, as expected for an ideal two-component mixture. Therefore, a model using $\lambda = 905$ nm was constructed. The standard error of estimate (SEE) with this model was 0.17% (w/w). The standard error of prediction (SEP) obtained from a cross validation estimate was 0.19% (w/w) ($R = 0.998$) (Figure 5).

is particularly broad due to the presence of two or more types of hydrogen bonded molecular complexes (28). In addition, weaker absorptions at 829 and 730 nm can be distinguished. The ethanol spectrum is more complex due to the presence of three near-IR-active functional groups (methyl, methylene, and hydroxide). The band at 905 nm is particularly important to this study and is assigned to the third overtone of the CH stretch on the methyl group. The shoulder at 935 nm is assigned to the third overtone CH stretch on the methylene group. The band at 960 nm is assigned to the OH stretch. This band becomes more evident when ethanol is diluted in carbon tetrachloride due to lack of hydrogen bonding. The first two assignments are consistent with those previously
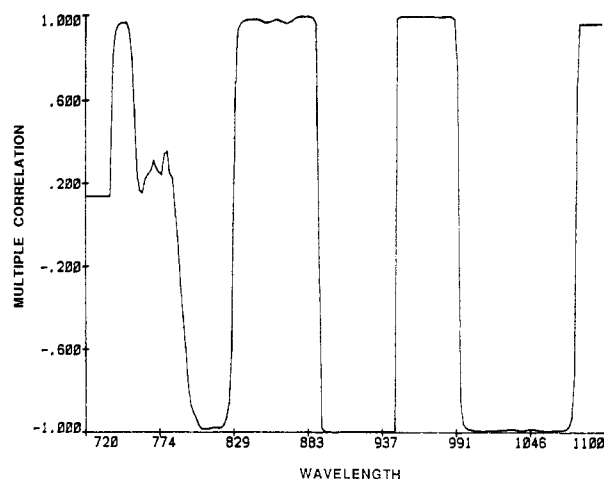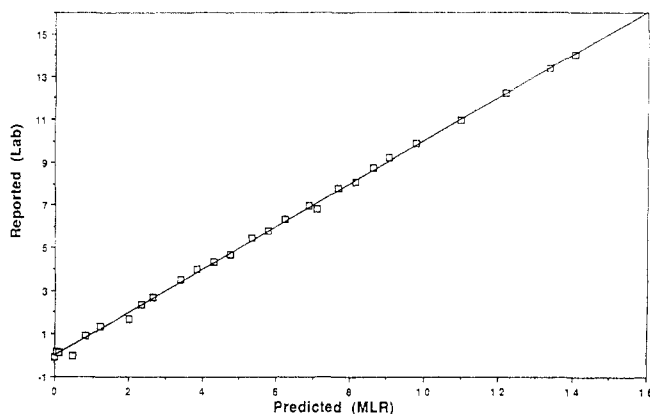
Figure 5. SEP correlation of water/ethanol mixtures using MLR and the 905-nm wavelength.

Effect of Light Scatter. During the time course of a fermentation, the number of yeast cells may increase by several orders of magnitude. This will result in greater light scattering, which may either increase or decrease the apparent absorbance through changes in the effective path length (30). This path length change could also affect ethanol determination. In order to investigate the influence of cell mass, a series of water/ethanol/yeast mixtures were analyzed in which the ethanol was varied between 0 and 7% (w/w) and the yeast concentrations varied between 0 and 17 g/L.

Figure 6A shows spectra recorded in a 1 × 1 × 4 cm cuvette in diffuse reflectance geometry. These spectra appear very similar to those recorded directly on the fermentation vessel (see Figure 9A). The major features are the water band at 960 nm and a decrease in relative absorbance baseline due to changes in yeast concentrations.

Figure 6B shows how the second derivative transformation corrects for baseline offset, and Figure 6C shows the second derivative difference, where a spectrum of a mixture containing no ethanol was subtracted from the set. Changes in the band at 905 nm with different ethanol concentrations are now clearly visible, while the overall change in the water band is due to displacement of water by yeast and ethanol. In fact, all spectra with pronounced changes in the 935-nm band correspond either to high yeast or high ethanol concentrations. These changes are not regular as in the fermentation spectra (compare Figure 9C) because ethanol and yeast are changing randomly with respect to each other. A one-wavelength (λ = 905 nm) model similar to that constructed for the ethanol/water solutions, but with different slope and offset, successfully predicts ethanol concentration despite the presence of yeast. This result is supported by the multiple R plot (Figure 7), which shows a good correlation in the spectral region corresponding to the methyl band.

However, the SEP of 0.27% (w/w) ($R = 0.980$) obtained from a cross-validation analysis was significantly greater than that of the ethanol/water mixtures (Figure 8). This is not entirely unexpected because the presence of these highly scattering organisms contribute considerable noise to the measurements.

Quantitative Determination of Ethanol in Fermentation. The production of ethanol in the medium defined in Table I was followed in real time. Spectra were taken at half-hour intervals for a 30-h period. A representative set of spectra is shown in Figure 9A. The most obvious change in the spectra is the decrease in relative baseline absorbance with increased time of the reaction. With increased scattering material, relative reflectance increases, causing more light to return to the detector (30), thus decreasing the relative absorbance. At the beginning of the fermenation, when yeast production is very slow, the baseline offset remains constant.
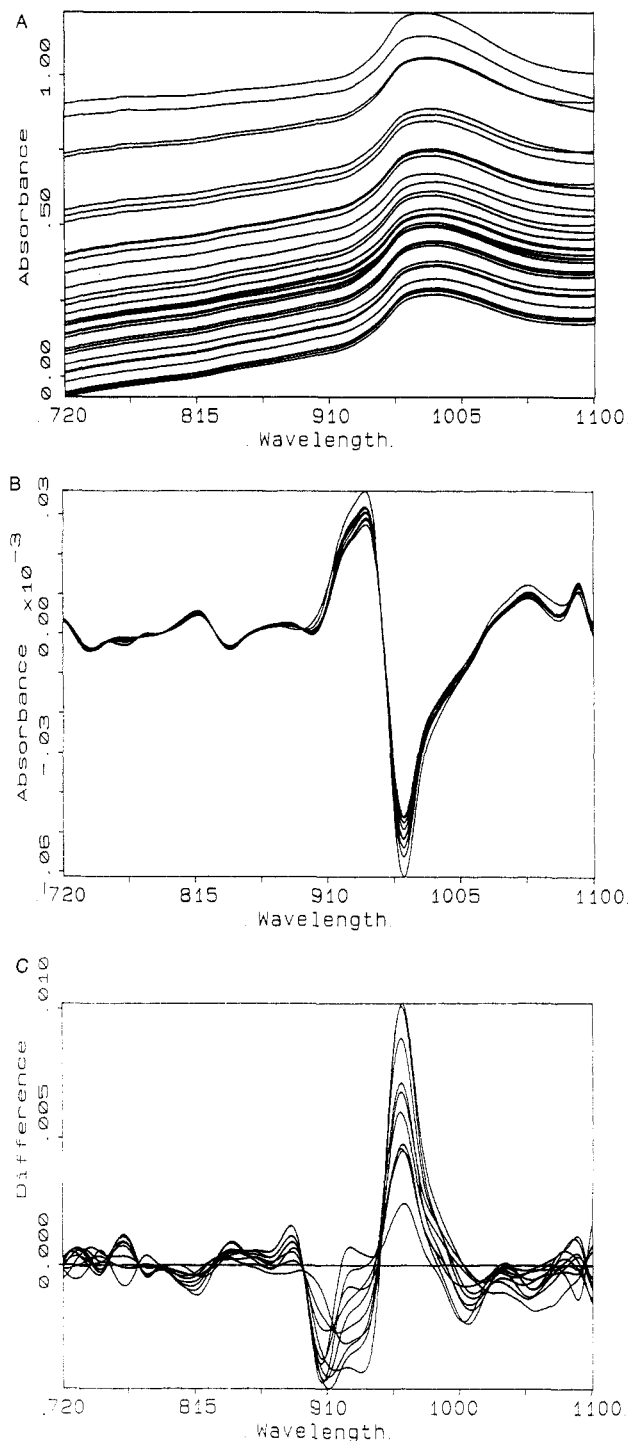

Figure 6. Absorbance spectra of water/ethanol/yeast mixtures: ethanol concentration 0–7% (w/w), yeast concentrations 0–17 g/L (A); second-derivative spectra of 7A (B), second-derivative spectra of 7B (C). Spectra taken in backscattering geometry.

However, as the yeast cells begin to rapidly reproduce, the baseline offset decreases, and when yeast reproduction stops, the offset again becomes constant. While there is no evident ethanol information in this set of spectra because of the baseline offset variation and the large size of the water peak, calculation of the second derivative enhances the third overtone methyl CH stretch (Figure 9B). Again, the spectral information is further enhanced by subtraction of a spectrum, from early in the fermentation process (Figure 9C). By comparing Figure 9C to Figure 3C and Figure 6C, it is evident that the signal to noise ratio (S/N) achieved in the fermentation broth is not as good as in the artificial mixtures. This is due in part to a greater extent of noise rising from stirring and
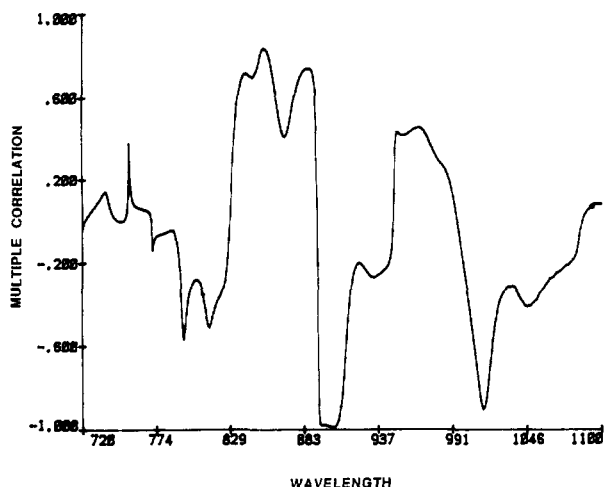
Figure 7. Multiple R plot vs wavelength of water/ethanol/yeast mixtures using one wavelength.
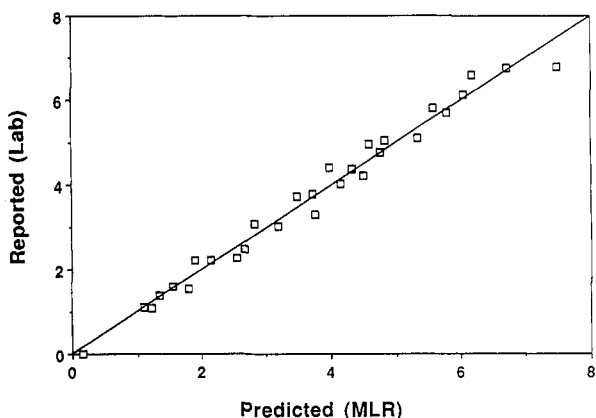

Figure 8. SEP correlation of water/ethanol/yeast mixtures using MLR and the 905-nm wavelength.

bubbling and in part to a reduced signal from the backscattered light compared to the transmission cell used for the ethanol/water experiments. Correlation between the GC reference analysis and the SW-near-IR second derivative spectra at 905 nm resulted in a SEE of 0.19% (w/w) (R = 0.993). A linear regression model was constructed by using a single wavelength (905 nm) of the second derivative spectra from this fermentation experiment as a calibration set. Prediction of ethanol production over the time course of the fermentation is shown in Figure 10. Also shown is the concentration of ethanol measured by GC on samples withdrawn from the reaction vessel immediately after the recording of a spectrum. The shape of this curve follows the ethanol production pattern of a typical batch fermentation (*31*).

Applicability of Calibration Constants to Succeeding Fermentation. The final series of studies was designed to investigate whether a model developed for one fermentation could be applied to succeeding runs. Accordingly, two further experiments were undertaken, which were reasonable duplications of the first. Figure 11 shows that the model developed on the first fermentation could be successfully applied to the second and third fermentations. The linear regression equation for the production of ethanol was

$$\% \text{ ethanol (w/w)} = K(0) + K(1) A_{2nd}(905) \qquad (1)$$

where $K(0)$ = 2.82 and $K(1)$ = -70888 and A_{2nd} is the second derivative absorbance value. The standard error of prediction was 0.42% (w/w) and R = 0.95. Conversely, models constructed with either the second or third fermentations could be used to predict the other two with similar values of SEP
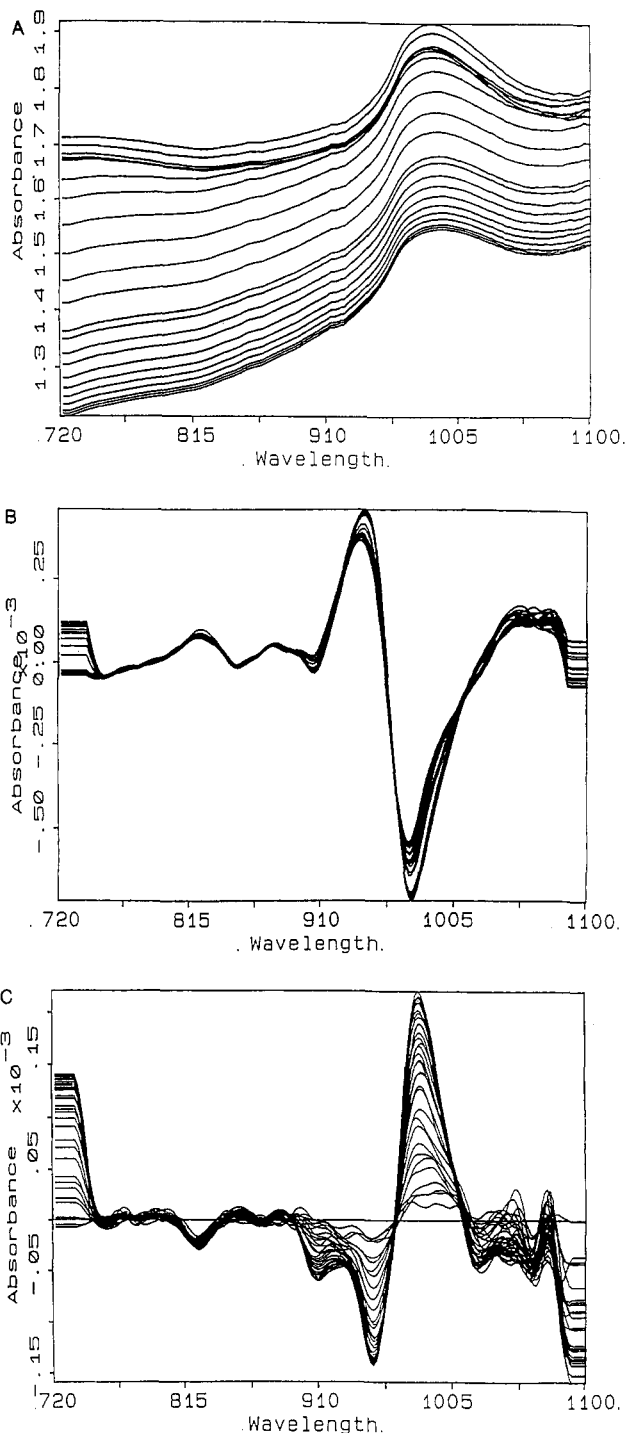

Figure 9. Absorbance spectra of fermentation over time (A). Second derivative spectra of 9A (B). Second derivative difference spectra of 9B (C). Spectra taken in backscattering geometry.

and R. These results are all the more remarkable when one considers that the probe was removed and replaced between each fermentation.

CONCLUSION

We have successfully demonstrated the potential of SW-near-IR spectroscopy for monitoring of a bioprocess for ethanol concentration. The major advantage of this technique is that it is noninvasive and requires only that the reactor vessel have a quartz or glass window. Thus, the need for elaborate sterile sampling systems and antifouling probes is eliminated. In its present form the cost of the instrumentation (~$10000) may seem high. However, inexpensive instruments based upon light-emitting diodes have been constructed for agricultureal
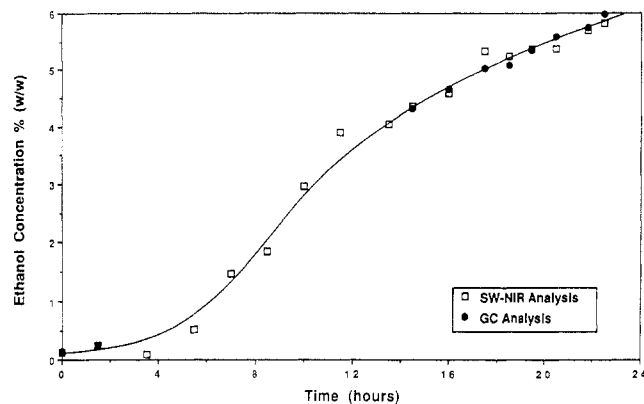
Figure 10. Prediction of ethanol production during the time course of a fermentation using the 905-nm second derivative wavelength value.
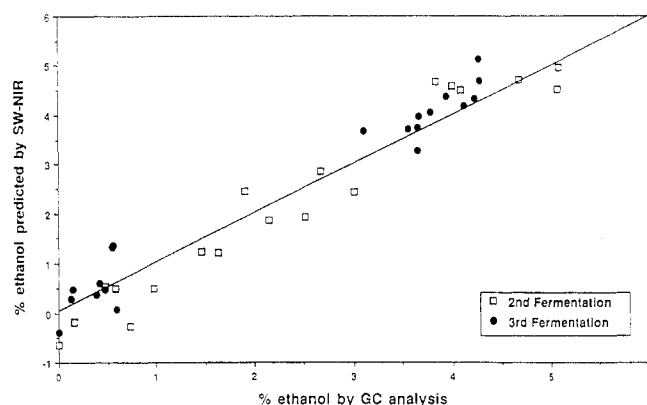

Figure 11. Prediction of ethanol content during other fermentations using SW-near-IR compared to GC analysis.

product analysis and could be adapted for use here (10). Another advantage of this approach is the apparent robustness of the calibration, as shown by the ability to apply a model developed on one fermentation to succeeding fermentations. This method represents an excellent tool for monitoring and control of ethanol production fermentations. However, the present technology does not yet allow monitoring of ethanol at trace level, as in the case of aerobic fermentations.

The current major drawback to the SW-near-IR method is its precision (SEP = 0.42%). While it is more reproducible than other reported spectroscopic methods (15, 19), the detection limits and precision of gas chromatography, flow injection analysis, and enzyme-based electrodes are superior and this may be of importance in certain applications. One of our research goals is to improve the S/N of our measurements and decrease detection limits proportionally.

The final advantage of our technique is the potential for simultaneous multiparameter analysis. Current research is directed toward demonstration of SW-near-IR methods for glucose, cell density, and aerobic/anaerobic status.

LITERATURE CITED

(1) Humphrey, A. E. *Chem. Eng.* **1974**, *81* (26), 98–112.
(2) Clark, D. J.; Calder, M. R.; Carr, R. J. G.; Blake-Coleman, B. C.; Moody, S. C. M.; Collings, T. A. *Biosensors* **1985**, *1*, 213–320.
(3) Dinwoodie, R. C.; Mehuert, D. W. *Biotechnol. Bioeng.* **1985**, *26*, 1060–1062.
(4) Alberti, J. C.; Phillips, J. A.; Fink, D. J.; Wacasz, F. F. *Biotechnol. Bioeng. Symp.* **1985**, *15*, 689–722.
(5) Callis, J. B.; Illman, D. L.; Kowalski, B. R. *Anal. Chem.* **1987**, *59*, 625A–637A.
(6) Mayes, D. M.; Callis, J. B. *Appl. Spectrosc.* **1989**, *43*, 27–32.
(7) Beebe, K. R.; Kowalski, B. R. *Anal. Chem.* **1987**, *59*, 1007A–1017A.
(8) Kelly, J. J.; Barlow, C. H.; Jinguji, T. M.; Callis, J. B. *Anal. Chem.* **1989**, *61*, 313–320.
(9) Phelan, M. K.; Barlow, C. H.; Kelly, J. J.; Jinguji, T. M.; Callis, J. B. *Anal. Chem.* **1989**, *61*, 1419–1424.
(10) Norris, K. H. *NATO Adv. Study Inst. Ser.*, **1983**, *46*, 471–484.
(11) Norris, K. H. *Biotechnol. Bioeng.* **1983**, *25*, 603–607.
(12) Official Methods of Analysis of the Association of Official Analytical Chemists; William Hormitz, Ed.; Association of Official Analytical Chemists: Washington, DC, 1980.
(13) Kovar, J. J. *Chromatogr.* **1985**, *333* (2), 389–403.
(14) Cutaia, A. J. *J. Assoc. of Anal. Chem.* **1984**, *67*, 192–193.
(15) Kuehl, D.; Crocombe, R. *Appl. Spectrosc.* **1984**, *38*, 907–909.
(16) Guillou, M.; Tellier, C. *Anal. Chem.* **1988**, *60*, 2182–2185.
(17) Buchanan, B. R.; Honigs, D. E.; Lee, C. J.; Roth, W. *Appl. Spectrosc.* **1988**, *42*, 1106–1111.
(18) Halsey, S. A. *J. Inst. Brew.* **1985**, *91*, 306–312.
(19) Gomy, C.; Jouan, M.; Quy Dao, N. *C. R. Hebd. Seances Acad. Sci.* **1988**, *306* (II), 417–422.
(20) Wiseman, A. *TrAC, Trends Anal. Chem.* **1988**, *7*, 5–7.
(21) Walters, B. S.; Nielsen, T. J.; Arnold, M. A. *Talanta*, **1988**, *35*, 151–155.
(22) Worsfold, P. J.; Ruzicka, J.; Hansen, E. H. *Analyst* **1981**, *106*, 1309–1317.
(23) Lazaro, F.; Luque de Castro, M. D.; Valcarcel, M. *Anal. Chem.* **1987**, *59*, 1859–1863.
(24) Martin, G. E.; Burggraff, J. M.; Dyer, R. H.; Buscemi, P. E. *J. Assoc. Off. Anal. Chem.* **1981**, *64*, 186–193.
(25) Owen, A. J. *The Diode-Array Advantage in UV/Visible Spectroscopy*; Hewlett-Packard Publication No. 12-5954-8912; Hewlett-Packard: Palo Alto, CA, 1988.
(26) Van Hare, D. R.; O'Rourke, P. E.; Prather, W. S.; Bowers, M. B.; Hovanec, M. J. *On-Line Fiber Optic Spectrometry*; Du Pont Publication DP-MS-88-186; Du Pont: Wilmington, DE, 1989.
(27) Sharaf, M. A.; Illman, D. L.; Kowalski, B. R. Chemometrics, In *Chemical Analysis: A Series of Monographs on Analytical Chemistry*; Elving, P. J., and Winefordner, J. D., Eds.; Kolthoff, I. M., Editor Emeritus; John Wiley and Sons: New York, 1986; Vol. 82.
(28) Scherer, J. R. In *Advances in Infrared and Raman Spectroscopy*; Clark, R. J. H., Hester, R. E., Eds.; Heyden: London, 1979; Vol. 5, Issue 3, pp 149–216.
(29) Weyer, L. G. *Appl. Spectrosc. Rev.* **1985**, *21*, 1–43.
(30) Reynolds, L.; Johnson, C.; Ishimaru, A. *Appl. Opt.* **1976**, *15*, 2059–2067.
(31) Wang, D. I. C.; Cooney, C. L.; Demain, A. L.; Dunnill, P.; Humphrey, A. E.; Lilly, M. D. *Fermentation and Enzyme Technology*; John Wiley & Sons: New York, 1979; p 79.